ARMA 13-224

Advances in Numerical Modeling of Microseismicity

Hazzard, J.H. and Pettitt, W.S.
Itasca Consulting Group, Minneapolis, MN, USA

This paper was prepared for presentation at the 47th US Rock Mechanics / Geomechanics Symposium held in San Francisco, CA, USA, 23-26 June 2013.

ABSTRACT: A simple technique is presented for extracting seismic information from slip on faults in distinct element models. It is shown that a simple static-dynamic friction law is sufficient to induce instability, and therefore produce seismic events. With this approach, all slips are seismic since the drop in frictional resistance is always faster than the drop in loading. In reality, not all events are seismic and the condition for instability depends on the system stiffness, fault roughness and normal stress. To simplify the problem, it is proposed that a user-defined minimum normal stress is required in the models for slips to be considered seismic. The method is shown to produce realistic behavior when simulating a laboratory experiment of slip on a single fault. A field-scale model with multiple intersecting faults is also presented. Seismicity is recorded and magnitudes are realistic, but more investigation is required before this method can be used in realistic field-scale modeling.

1. INTRODUCTION

Extracting seismic information from numerical models is useful for several reasons. Comparing modeled seismicity (location, magnitudes and mechanisms) to seismicity recorded in the field provides a potential method to help calibrate the models. The models can also be used to help understand the mechanisms behind the observed seismicity (e.g., slip on an existing fault versus opening of a new fracture). For example, it even has been shown that the magnitude distribution of seismicity can give clues about the nature of hydraulic fracturing [1]. Understanding and modeling these relationships potentially can improve the efficiency of hydraulic fracturing operations.

A rich body of research exists on the modeling of global scale earthquakes. These models generally involve simulation of a single fault or fault system using complex friction laws [2] or even a finite thickness of gouge material [3]. The seismicity resulting from a continuously yielding joint model is described in [4], and the implementation of a rate-state friction law in distinct element models is described in [5].

In geomechanics applications, it is expected that there will be hundreds to thousands of events and the level of detail and rigor in global earthquake analysis is generally not necessary or feasible. In addition, practitioners rarely know the values of the various parameters involved in correctly implementing these complex laws.

This paper will describe a simple approach to extracting seismic information from slip on pre-existing joints in discontinuum numerical models. It is also possible to obtain seismic information from formation of new fractures in intact rock material [6, 7]; however, there is evidence that the majority of seismicity recorded in hydrofracture operations is due to slip on existing faults. It will be shown that realistic magnitudes and magnitude distributions can be obtained even for these simplified approaches to modeling seismicity.

2. SEISMIC SLIP

2.1. Theory

Sudden slip can occur on a joint or fault if two conditions are met:

1. There is a variation in frictional resistance during sliding; and
2. The frictional resistive force decreases faster than the unloading of the medium surrounding the fault.

The concept is usually illustrated by considering a spring pulling a sliding block (Figure 1). The force increases as the spring is pulled until the frictional strength is overcome. The frictional strength then decreases and the spring unloads. If *F* falls off faster than *K*, the block will accelerate. Eventually *F* becomes greater than the force in the spring, and the block decelerates coming to an eventual stop.

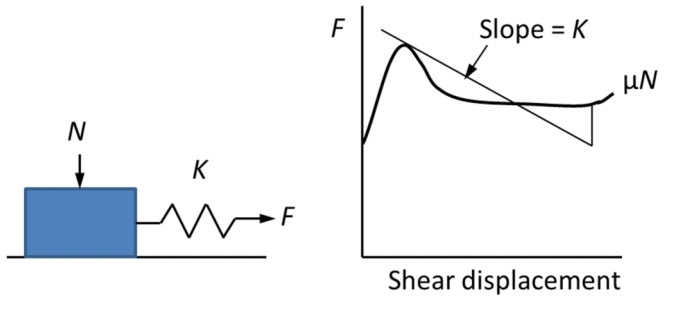

Figure 1. Spring slider model to illustrate seismic slip.

As mentioned above, various complex frictional laws exist to describe the change in friction with slip or velocity. The simplest approach would be to consider a static-dynamic friction law such that the friction drops instantly from a high static value to a low dynamic value when the frictional strength is exceeded. This would be successful in producing instability, but in this case, every slip event would be seismic. In reality, aseismic slip will occur in many instances. The transition from stable to unstable slip depends on [8]:

i. Normal stress;

ii. System stiffness; and

iii. Fault surface roughness.

Low stiffness, high normal stress and smoother joints favor instability. This will be discussed further in Section 4.

2.2. Geomechanical Modeling

In geomechanical modeling, two simplifications are usually made:

1. Models are run pseudo-statically so that energy is damped and solution is reached more quickly; and
2. Faults and joints are assigned constant friction coefficient.

What is the effect of these assumptions on the seismic behavior of joints? In a pseudo-static model, there is no overshoot, so the slip will stop when the resisting stress is equal to the unloading stress. This is probably not critical and will result only in events with smaller observed slip magnitudes.

If friction is held constant, then there is no stress drop and essentially there is no seismic event at all. Some researchers have related slip distance or frictional energy to seismicity from these types of models [9]. The problem with this approach is that joints tend to slip continuously and there is no clear demarcation of separate events. Therefore, it is difficult to relate model results to observed locations and magnitudes in the field. These different modeling approaches are examined for a simple test in the next section.

3. SIMULATION OF LABORATORY SLIP EXPERIMENT

3.1. Description of experiment

In the early 1980s, a series of experiments were conducted on a large block of granite to observe the mechanics of fault slip under different conditions [10]. The sample of Sierra gray granite was 150 x 150 x 40 cm, sawed diagonally in half to simulate a fault. Then, it was deformed in a biaxial rock press at normal stress up to 6.41 MPa. Strain gauges and velocity transducers were mounted along the top of the fault surface. Local shear stresses were calculated from the strains assuming elastic deformation of the blocks. An example slip event is shown in Figure 2.

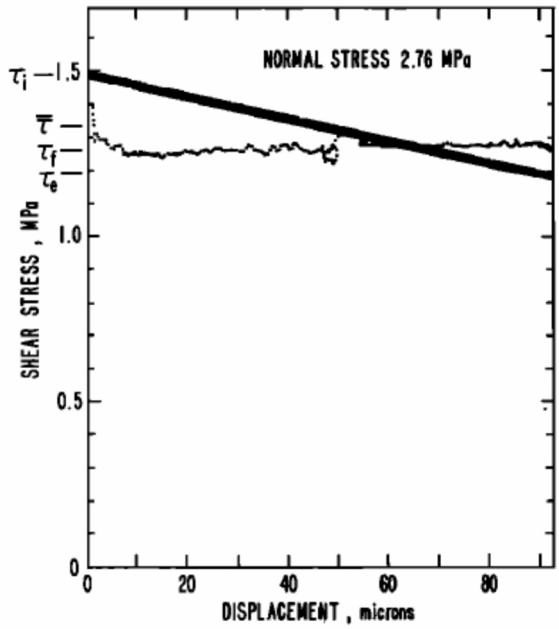

Figure 2. Local shear stress versus displacement for a stick slip event at σ_n = 2.76 MPa. The heavy diagonal line of slope 33 MPa/mm is the unloading curve of the press. Reproduced from [11].

3.2. Model Setup

A numerical model of the experiment was created using *3DEC* [12]. The model consists of two blocks discretized into tetrahedral zones. This is a distinct element program meaning that the blocks are free to move, rotate and separate relative to one another. It also uses an explicit calculation scheme so information

propagates through the model dynamically. Normal and shear forces are calculated at each contact and then are used in the calculation of block motion. Contacts exist between the two blocks at each node.

The properties of the model are given in Table 1. The actual granite used in the experiment is stiffer (shear modulus = 25 GPa); however, in the *3DEC* model, boundary conditions are applied directly to the rock so it is as if there is an infinitely stiff loading frame. This was not the case in the lab experiment, so the stiffness of the *3DEC* model was reduced to more closely mimic the stiffness of the rock + loading frame from the experiment. The peak and residual friction angles were derived from the peak and residual shear stress in Figure 2. The model is shown in Figure 3.

Table 1. Properties of the model.

Property	Value
Rock Young's Modulus, E	10 GPa
Rock Poisson's Ratio, ν	0.25
Joint normal stiffness, k_n	600 GPa
Joint shear stiffness, k_s	600 GPa
Joint friction angle (static), ϕ_s	28.5°
Joint friction angle (dynamic), ϕ_d	24°

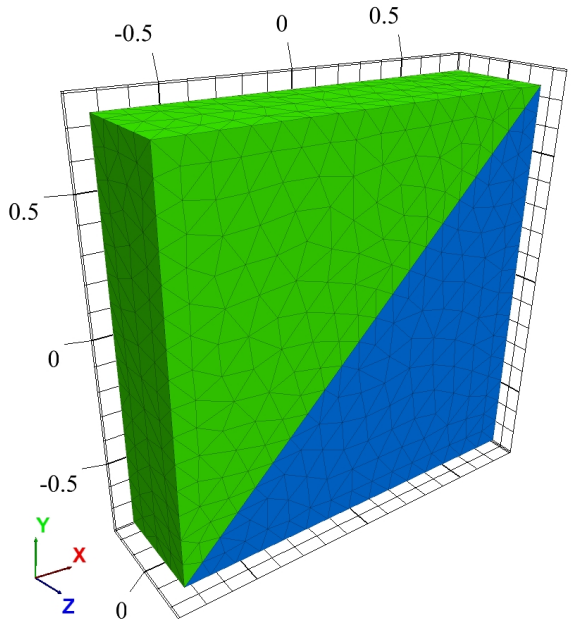

Figure 3. Distinct element model of laboratory slip experiment.

The model is first loaded to a normal stress of 3 MPa by moving the four outer rectangular boundaries inwards at a constant velocity (the triangular faces on the front and back are free from boundary conditions). Once the desired normal stress is reached, the velocity of two of the walls is reversed to start increasing shear stress while maintaining a constant normal stress. Stresses and displacements at points on the fault surface were monitored throughout the test.

To simulate variation in frictional resistance during sliding, the simplest possible approach was adopted. A static-dynamic friction law was applied such that the friction on the fault dropped from the peak (static) value to the residual (dynamic) value instantaneously when the frictional resistance is exceeded. If the shear stress then drops below the maximum frictional resistance, the contact stops sliding and the friction angle increases back to the peak value. This is summarized in Eq. (1).

$$\begin{aligned} \pm_s &\geq \pm_n \tan ¤_s \quad , ¤ \rightarrow ¤_d \\ \pm_s &< \pm_n \tan ¤_d \quad , ¤ \rightarrow ¤_s \end{aligned} \tag{1}$$

Where σ_n is the normal stress on the fault and σ_s is the shear stress.

3.3. Dynamic Model

The model was run dynamically with very little damping. A history of shear stress versus shear displacement for a point on the middle of the fault is shown in Figure 4. You can see how shear stress initially accumulates with little displacement when the fault is not slipping (the fault itself has a finite stiffness, so the shear displacement during this stage is not zero). When the frictional strength is exceeded, the friction angle is set to the residual value and the shear stress drops. The blocks then quickly slide past each other until the loading falls below the resisting stress. The blocks continue to slide briefly as they decelerate (recall this is a dynamic simulation) and then eventually come to rest after about 98 μm of slip. The friction then recovers to the peak (static) value. The slope of the unloading curve is equal to the shear modulus of the material (4 GPa) divided by some function of the block and fault dimension. For this model, we will assume ~1 m.

After the fault stops slipping, there is a small decrease in shear stress and displacement due to dynamic vibration of the system. The shear stress then increases again until the peak frictional strength is exceeded again and slip starts again. Subsequent slip events are not as large as the first. This is because the subsequent slips are more localized, whereas the first slip involves activation of the entire fault (see Figure 5).

In general, even for this simplified friction law, the system behaves similarly to that of the actual laboratory experiment (compare to Figure 2).

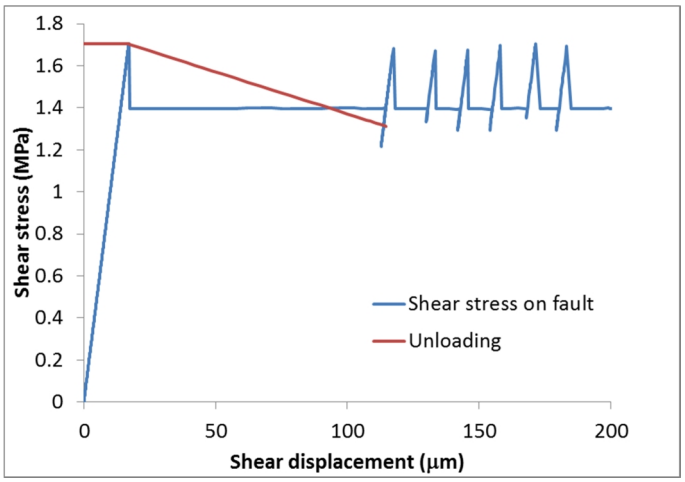

Figure 4. Shear stress versus shear displacement for a point in the middle of the fault (dynamic simulation). The normal stress is constant at 3MPa. The slope of the unloading curve is -4.0 GPa/m.

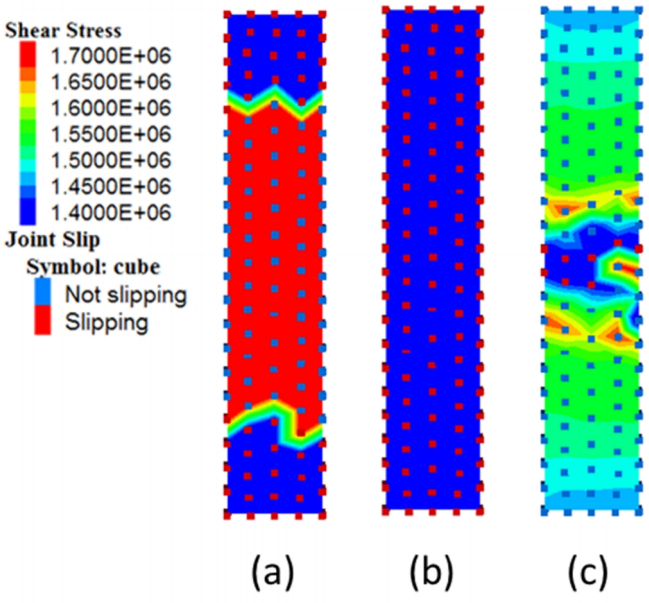

Figure 5. Shear stress and slip on the fault (a) just before the first slip event (b) during the first slip event, (c) during the second slip event.

3.4. Seismic magnitudes

The seismic moment is a measure of the size of an earthquake and for shear events the definition is

$$M_0 = \mu A \Delta u \quad (2)$$

where μ is the shear modulus, A is the fault area and Δu is the slip displacement. The moment magnitude can then be defined by [13]

$$M_w = \frac{2}{3}\log M_0 - 6 \quad (3)$$

Assuming the moment is of units N·m. for the event of Figure 4, μ = 4 GPa, A = 0.85 m^2 and Δu = 97.6 μm. Using these values in Equations 2 and 3 gives a magnitude of M_w = -2.3. This is a bit lower than the magnitudes calculated in [13] for the laboratory study ($M_w \approx$ -1.8). This is because the shear modulus for rock was used to calculate moments in [13], whereas the actual rigidity of the system was probably less due to the finite stiffness of the loading frame.

We can examine the energy budget for the first slip event. The different energy quantities are shown in Figure 6. The energies are dominated by the strain energy decrease in the block, and the energy lost due to friction. The values are tabulated in Table 2. The energy imparted to the system by the boundaries is assumed to be negligible during the event due to the slow loading rate.

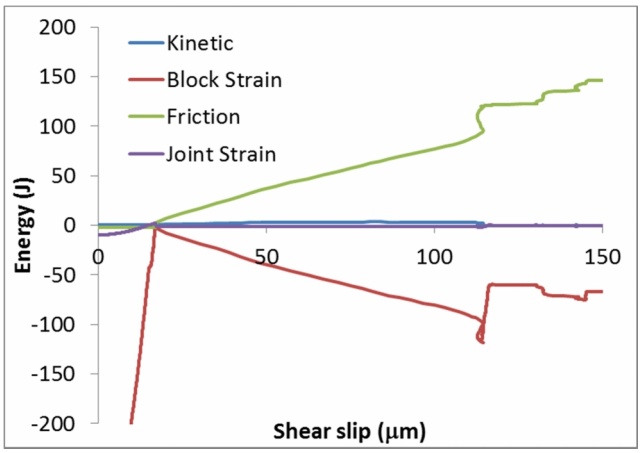

Figure 6. Energy quantities in the dynamic model. Values represent the change in energy from the start of the first slip event.

Table 2. Energy changes during the first slip event.

Energy Quantity (change)	Value (J)
Strain in rock	99.5
Strain in joint	1.7
Friction	95.6
Kinetic	3.5

Assume that the energy released by the slip event is related to the change in strain energy (rock + joint), E = 101.2 J. An empirical equation for energy magnitude is described in [14]:

$$M_e = \frac{2}{3}\log E - 3.2 \quad (4)$$

if E is in Joules. This yields an energy magnitude for this event of M_e = -1.9. The agreement is not bad considering that Eq. (4) was derived for large global earthquakes and may not be totally applicable to smaller events.

Interestingly, the ratio of kinetic energy change to strain energy change is ≈ 3.5%. This ratio (seismic efficiency) is similar to values obtained by [13] for an array of laboratory and mining scale events (efficiency < 6%).

3.5. *Pseudo-Static Model*

The same model was run with a large amount of numerical damping. Running the model pseudo-statically in this way is standard practice in most analyses because the models are much more computationally efficient. The shear stress versus shear displacement plot for the pseudo-static model is shown in Figure 7. This plot shows similar behavior to the dynamic case except that there is no overshoot so the shear displacement is only about 80% of the displacement in the dynamic case. This yields a moment magnitude of M_w = -2.4 (compare to -2.3 in the dynamic case).

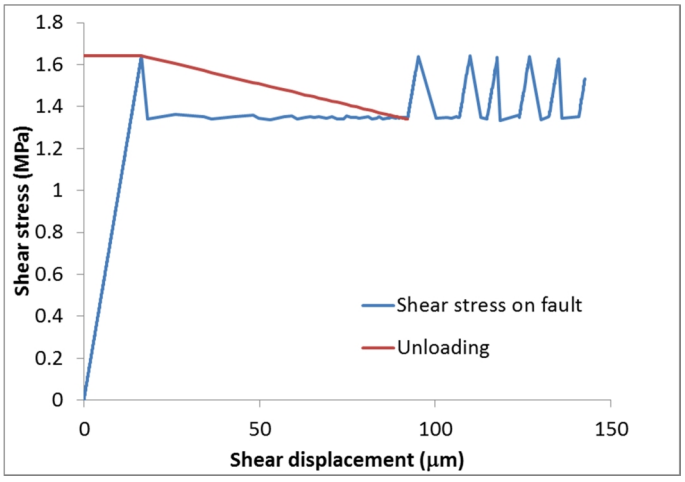

Figure 7. Shear stress versus shear displacement for a point in the middle of the fault (pseudo-static simulation).

3.6. *Constant Friction*

It is common in practice to run models assuming a constant friction on the faults. This was done for this example and the result is shown in Figure 8. The joint reaches a state of stable sliding. There is no energy release and it is not possible to determine the end of the event. It is therefore not possible to compute a magnitude for this event.

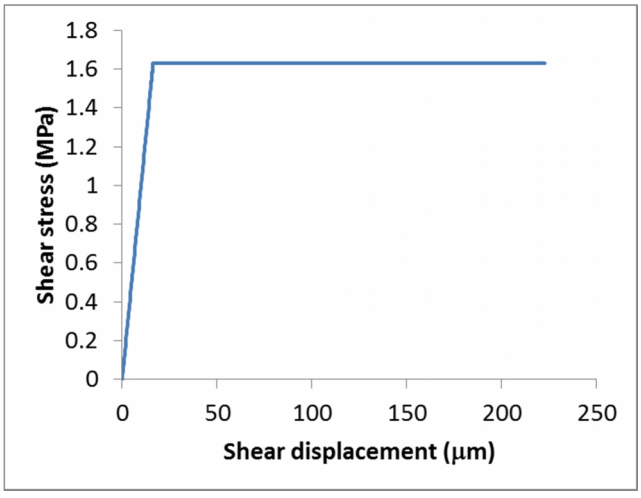

Figure 8. Shear stress versus shear displacement for a point in the middle of the fault (pseudo-static simulation with constant friction).

4. SEISMICITY IN FIELD-SCALE MODELS

4.1. *Method*

In the previous example, it was assumed that the initial slip was a single large event. In field scale models, there will likely be hundreds or thousands of intersecting faults with various parts slipping at various times. How can we extract seismic information from these models?

One problem with the simple static-dynamic friction law is that all slips are seismic since the drop in frictional strength will always be faster than the drop in loading. In Section 2, it was shown that the stability depends on the system stiffness, the fault roughness and the normal stress. For simplicity, assume that the stiffness and fault roughness will not vary significantly across the area of interest. The condition for stability is then simply a function of the normal stress. We propose a user input, $\pm_n^{\min}$, that is the minimum normal stress for which a slip can be considered a seismic event. Enforcing a minimum normal stress for seismic events had the added practical benefit of limiting the number of seismic events recorded.

The second problem is how to separate events in space and time. It is assumed that if there are two slipping contacts, they will be considered only part of the same event if they lie on the same fracture plane. They will also be considered only part of the same event if they are within some small distance of each other on that plane. This minimum distance is also a user input called x_{min}.

It may seem logical that only adjacent slipping contacts should be considered part of the same event; however, experience has shown that it is very common for slip to jump over a contact that starts slipping later. It is obvious that these should all be part of the same event so in general, x_{min} should be set higher than the average contact spacing.

For an event composed of multiple slipping contacts, the moment then is calculated from the total contact area times the average contact shear displacement times the average shear modulus of the surrounding material

$$M_0 = \frac{1}{n^2}\sum_{i=1}^{n} \mu_i A_i \Delta u_i \quad (5)$$

where n is the number of contacts that make up the event. Note that μ_i refers to the shear modulus of the rock surrounding the contact, not the joint shear stiffness. The moment magnitude then is calculated from Eq. (3).

In summary, the algorithm for recording seismicity is as follows.

1. A contact starts slipping. The friction drops to the dynamic value.
2. If the normal stress on the contact is less than $\pm_n^{\min}$ (compression positive), then it is ignored.
3. If the contact lies on the same fracture plane as another slipping contact and is within x_{min} of another slipping contact, then the new slipping contact is subsumed into the existing event. If not, a new event is formed.
4. When a contact stops slipping, the friction is set to the static value. If all contacts in an event have stopped slipping, it is considered inactive and the moment and magnitude are calculated.

Note that this does not consider the case where two separate slip events grow together. Figure 9 shows the algorithm applied to the example of Section 3 using x_{min} = 23 cm (twice the average contact spacing) and $\pm_n^{\min}$ = 0.1 MPa. The value for x_{min} was chosen based on observations that large slip events had a tendency to skip over some contacts. Therefore an x_{min} of twice the contact spacing ensured the slips would all be considered part of the same event. The choice for $\pm_n^{\min}$ was fairly arbitrary. In this example it does not make much difference but in the field-scale example of the next section, the choice of $\pm_n^{\min}$ is important. Guidelines for choosing this value are given in the next section.

Figure 9 shows that the first slip event resulted in two seismic events being recorded with magnitudes of -2.4 and -2.6, compared to the single event of magnitude -2.3 assumed in the analysis of Section 3. The sum of the moments of these two events is very similar to the moment calculated for the single event in Section 3.4. It would be possible to combine events that grow together with a post-processing step, however in field-scale models, the faults will be confined so it is unlikely that slip events will start at the edges and grow towards the middle as with this event.

The right side of Figure 9 shows a series of smaller events representing the localized slips that occurred after the initial main event.

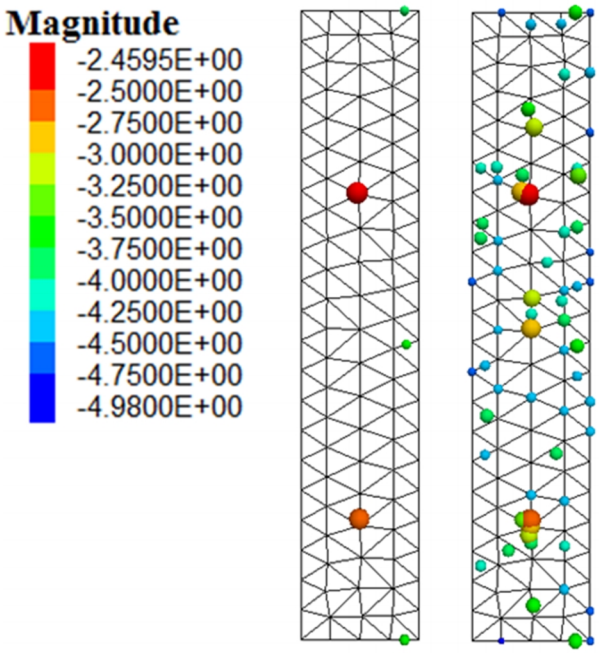

Figure 9. Seismic events recorded for the laboratory simulation of Section 3 after (left) 115 μm of slip, (right) 200 μm of slip.

4.2. Example

A 100 × 100 × 100 m cubic model was created to test the algorithm on a field-scale model. A set of circular fractures was inserted into the model with the properties shown in Table 3.

Table 3. Properties of the fracture set.

Property	Value
Size distribution	Gaussian
Mean radius	50 m
Standard deviation in radius	10 m
Minimum radius	5 m
Maximum radius	100 m
Orientation distribution	Random uniform
Position distribution	Random uniform
P32 (area of fracture per unit volume)	0.1 m^{-1}

The model was created first by generating the intact block. The fracture network then was generated with dimensions twice as large as the block. This was done to ensure that fractures with centers outside of the block, but extending into the block, would be considered. Blocks then were cut by the fractures. Since a block cannot be partially cut, sections of the cut planes lying outside of the circular fractures were bonded. Figure 10 illustrates the procedure.

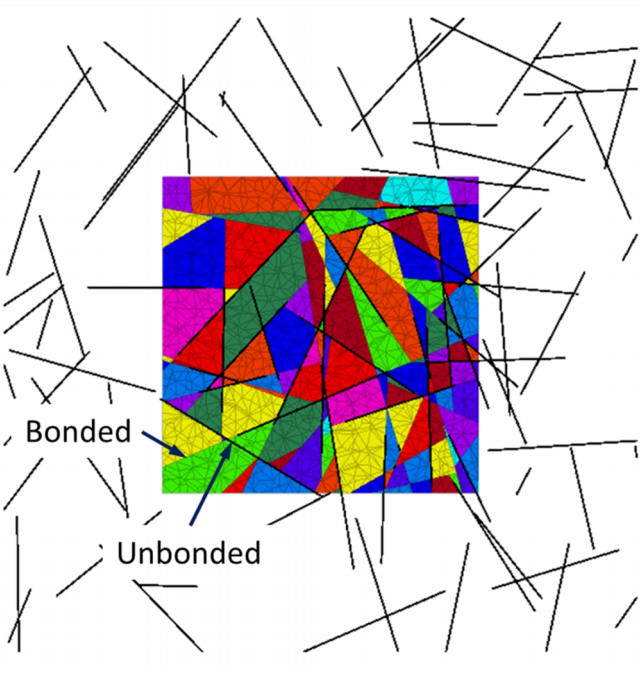

Figure 10. A 2D slice showing fracture network (black lines) and resulting blocks.

The properties of Table 1 were applied to the model rock and fractures. An initial isotropic compressive stress of 10 MPa was applied to the model. A constant stress of 10 MPa then was applied to the vertical edges, and a constant inward velocity was applied to the top and bottom walls to increase the stress in the vertical direction.

The seismic recording parameters were set to x_{min} = 10 m (twice the average contact spacing) and $\pm_n^{\min}$ = 0.8 MPa (10% of the average contact normal stress). The choice of $\pm_n^{\min}$ was again fairly arbitrary. One could establish the most appropriate value for $\pm_n^{\min}$ by performing a sensitivity study in which $\pm_n^{\min}$ is varied and the *b*-value is calculated (see below). It is expected that smaller values of $\pm_n^{\min}$ will result in smaller *b*-values because there will be more small events recorded.

The model was loaded to a vertical stress of 20 MPa and the resulting seismicity is shown in Figure 11. A total of 5800 events were recorded ranging in magnitude from -5.4 to -1.4; a realistic range for a volume of this size.

The spatial distribution shows clear linear features. These are the intersections of faults. More investigation is required to determine why these events seem to dominate.

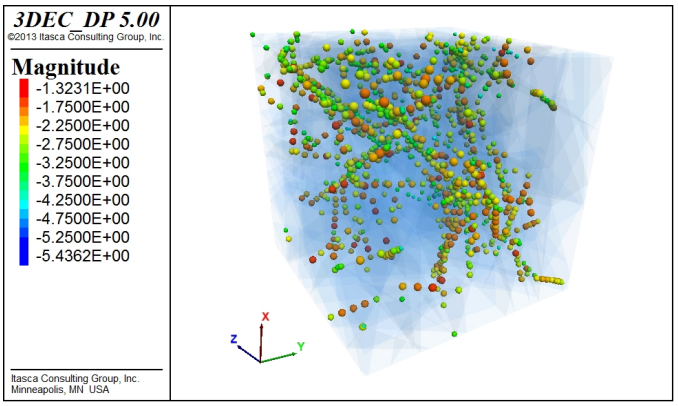

Figure 11. Seismicity recorded in field-scale model loaded to a vertical stress of 20 MPa.

The magnitude distribution is shown in Figure 12. In the field, the plot of number of events (logarithm) versus magnitude tends to produce a straight line with a slope close to 1. The plot in Figure 12 does not show a clear straight-line relationship. The number of events tends to decrease sharply for magnitudes greater than -2. This suggests perhaps that the size of the events is limited by the sample size (or equivalently, that the discretization of the sample is too coarse, meaning that there are not enough small events relative to the large events). More tests are currently being conducted on higher resolution samples under different loading scenarios.

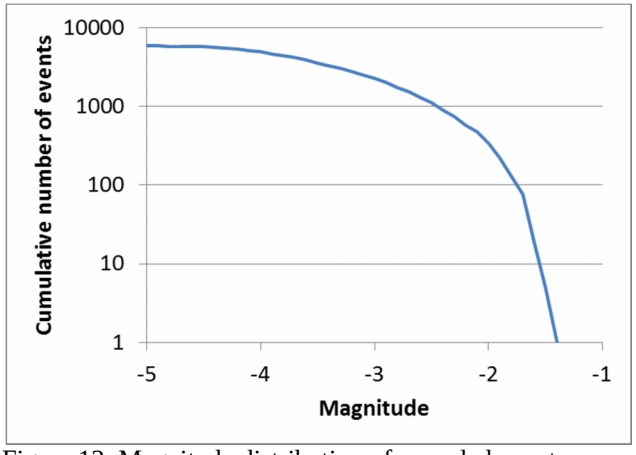

Figure 12. Magnitude distribution of recorded events.

5. CONCLUSIONS

A simple scheme is presented that will simulate seismicity due to slip on faults in a distinct element model. It was shown that a simple static-dynamic friction law is capable of producing instability (seismicity) even if the model is run pseudo-statically. The main problem is that with this approach, all slips are seismic, whereas in reality many are not. It is proposed that a minimum normal stress is required for a slip to be considered seismic.

The method works well for seismicity on a single fault; however, some challenges need to be overcome when applying this approach to a field-scale model. Some research needs to be done to examine why the majority of events occur at fault intersections. Another problem is that in higher resolution models, potentially a very large number of events may be recorded and the data management will become unwieldy. Modifications may be required to limit the number of recorded events, such as enforcing a minimum duration or slip distance. Research on this is continuing.

REFERENCES

1. Scholz, C.H.. 1998. Earthquake and friction laws. *Nature* 391: 37–42.
2. Mora P. and D. Place, 1998. Numerical simulation of earthquake faults with gouge: Toward a comprehensive explanation for the heat flow paradox, *J. Geophys. Res.*, 103 (B9): doi:10.1029/98JB01490.
3. Cundall, P.A. and J.V. Lemos, 1990. Numerical simulation of fault instabilities with a continuously-yielding joint model, in *Rockbursts and Seismicity in Mines*, ed. C. Fairhurst, 147-152.
4. Lorig, L.J. and B.E. Hobbs, 1990. Numerical modeling of slip instability using the distinct element method with state variable friction laws, *Int. J. Rock Mech. Min. Sci*.: 27, 525-534.
5. Hazzard J.F. & Young, R.P. 2000. Simulating Acoustic Emissions in Bonded Particle Models of Rock, *Int. J. Rock Mech. Min. Sci*.: 37, 867-872.
6. Tang, C.A. & Kaiser, P.K. 1998. Numerical Simulation of Cumulative Damage and Seismic Energy Release during Brittle Rock Failure—Part I: Fundamentals, *Int. J. Rock Mech. Min. Sci*.: 35, 113-121.
7. Dieterich, J.H., 1979. Modeling of rock friction 1. Experimental results and constitutive equations, *J. Geophys. Res.*, 84 (B5): 2161-2168.
8. Last N.C. and T.R. Harper, 1990. Response of fractured rock subjected to fluid injection part I. Development of a numerical model, *Tectonophysics*, 172: 1-31.
9. Okubo, P.G. and J. H. Dieterich, 1981. Fracture energy of stick-slip events in a large scale biaxial experiment, *Geophys. Res. Lett.*, 8: 887-890.
10. Lockner, D.A. and P.G. Okubo, 1983. Measurements of frictional heating in granite, *J. Geophys. Res.*, 88 (B5): 4313-4320.
11. Itasca Consulting Group, 2013. 3 Dimensional Distinct Element Code, Version 5.0, Minneapolis, MN, USA.
12. McGarr, A., 1994. Some comparisons between mining-induced and laboratory earthquakes, *Pure and Applied Geophysics*, 142: 467-489.
13. Scholz, C. 1990. *The Mechanics of Earthquakes and Faulting*, Cambridge University Press, Cambridge, U.K.